Int J Adv Manuf Technol (2018) 94:4543–4551
https://doi.org/10.1007/s00170-017-1181-5

ORIGINAL ARTICLE

Investigation on the effect of ball burnishing on fracture toughness in spiral API X70 pipeline steel

A. Bounouara[1] · **H. Hamadache**[2] · **A. Amirat**[2]

Received: 15 June 2017 / Accepted: 27 September 2017 / Published online: 8 October 2017

Abstract The present work is an investigation on the effect of mechanical surface treatment using ball burnishing technique on fracture toughness in spiral API X70 pipeline steel. The burnishing operation has been carried out on three series of impact API 5L 45 Ed specimens that have been prepared according to the location of the notch towards the weld bed: BM notched specimens, FZ notched specimens, and HAZ notched specimens. In the untreated specimens, the absorbed energy in BM specimens is higher than the energy found in FZ and HAZ through the testing temperature range of 50 to −40 °C. In surface-treated specimens, there has been a significant change in the three curves of absorbed energy versus temperature. This is observed when testing temperature decrease from 20 to −40 °C since the energy in BM specimens dropped drastically reaching values lower than that obtained for FZ and HAZ specimens. At the temperature range 50 to 20 °C, the absorbed energy in ball-burnished specimens is relatively higher. At lower testing temperatures below −40 °C, the absorbed energy converged to the same value. At room temperature, hardness tests indicate that where the absorbed energy is higher, hardness is lower.

Keywords Pipeline · steel · API X70 · burnishing · fracture · toughness

✉ A. Bounouara
abdelouaheb_b@yahoo.fr

[1] Mechanics of Materials and Plant Maintenance Research Laboratory (LR3MI), Faculty of Engineering Sciences, Badji Mokhtar University Annaba, Annaba, Algeria

[2] Research Laboratory of Advanced Technology in Mechanical Production, Faculty of Engineering Sciences, Badji Mokhtar University Annaba, Annaba, Algeria

1 Introduction

High-strength low-alloy (HSLA) API X70 steel is extensively used because there is a great demand either in replacing old and corroded pipes or in construction of new routes for conveying gas specifically in moderate-climate regions where the temperature drops rarely to −20 °C [1]. In addition, API X70 steel is well appreciated for its potential advantages including good combination of strength and toughness, good weldability, and low ductile to brittle transition temperature. However, failures in pipelines are still occurring despite the great effort invested in making them secure and reliable. The main failure mode is leakage or fracture induced by cracks and manufacturing defects in the pipes because of the production process [2–4]. The latter usually involves spiral rolling of laminated sheet metal and welding creating a weak link in pipelines because of the inherent characteristics of the weld process. The toughness value is therefore dependent on the location of the weld seam in the pipe, characterized by three zones: the base metal (BM), the fusion zone (FZ), and the heat-affected zone (HAZ). Since then, there are many researchers investigating the behavior of fracture toughness in pipeline steels [5–10].

Mechanical surface treatment by applying some minor plastic deformation on the superficial layers of a structure is another way of improving the lifetime of structure. One of the most interesting techniques in mechanical surface treatment is ball burnishing that is getting to be commonly used in the last few years [11–16]. The process has been used to impart certain physical and mechanical properties, such as appearance [17, 18], corrosion, friction, wear [19, 20], and fatigue resistance [21, 22]. Moreover, investigation concerns development of the technique, method of assessment, and computing tools in various materials and use conditions [23–26].

Table 1 Chemical composition of API 5L X70 steel in weight %

Element	C	Si	Mn	Al	Nb	V	Ti	Ni	Cu	Cr	Mo	Fe
(%)	0.07	0.37	1.54	0.04	0.05	0.084	0.005	0.028	0.014	0.027	0.004	97.7

Table 2 Specific mechanical properties of API 5L X70 pipeline steel

Requirements	E (GPa)	$\sigma_{y0.5}$ (MPa)	σ_{ts} (MPa)	A (%)
API X 70	190–220	485–635	531–758	22

The present work is a new investigation on fracture toughness of HSLA steel pipeline by introducing a burnishing operation on impact specimen. The main objective is to examine the response of mechanical surface treatment on fracture toughness in the three zones characterizing a weld bed in a spiral steel tube. A purpose ball burnishing device has been designed in order to carry out the mechanical surface treatment on impact specimens.

2 Experimental procedure

2.1 Material

API 5L grade X70 steel produced in spiral weld pipe mill unit of the steel complex of El-Hadjar, Algeria, is used. The chemical composition obtained by a diffractometry corresponded to that recommended by the standard API 5L as shown in Table 1, and the specific properties are given in Table 2.

2.2 Mechanical properties

2.2.1 Tensile tests

Two series of tensile tests have been carried out at room temperature, on a universal MFL VHP type hydraulic Zwick machine using a API 5L standard specimen. The first series consisted of three tensile specimens prepared from the base material (BM) as shown on Fig. 1a, b. The second series of three welded specimens has been carefully prepared from a steel sheet, cut from the tube as to get the weld bed within the central of the gauge length of the tensile specimen (Fig. 1c, d). The sheets have been first cut by means of a welding cutting torch from the tube, then flattened on a press machine. Then, specimen blanks have been saw cut at least 50 mm away from the border of the flattened steel sheets as to avoid the effect of the cutting heat. Tensile specimens have been machined on a horizontal milling machine.

2.2.2 Impact V-notch tests

Impact tests have been carried out on a 300-J Charpy machine, using standard Charpy V-notch specimens. Specimens were prepared from a steel sheet cut from a tube (Fig. 1). A great care has been taken in machining the impact specimens from the parent tube in order to locate the V-notch towards the

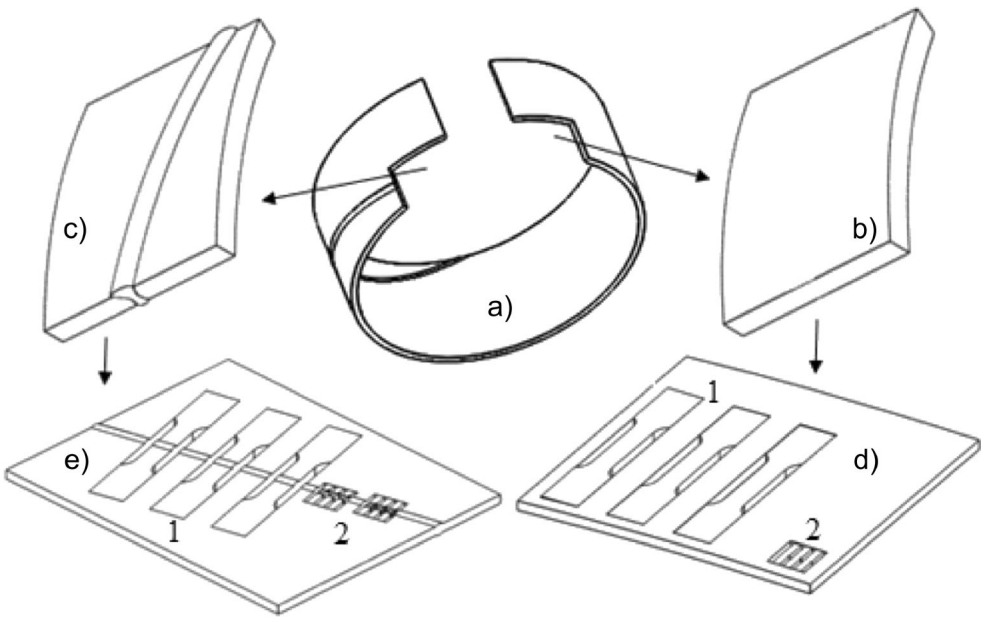

Fig. 1 Specimen preparation from 1219-mm-diameter tube made of API 5L X70 steel. 1 Tensile specimens; 2 impact specimens

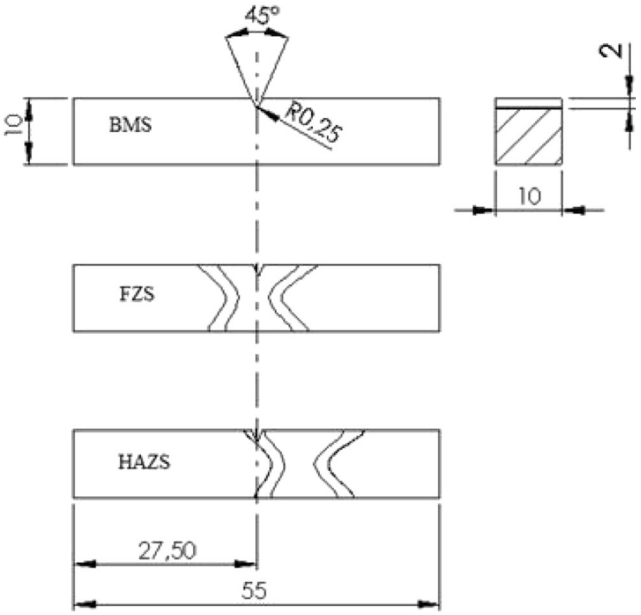

Fig. 2 Location of V-notch in impact specimens towards the weld bed

welding bed. Therefore, three types of specimens have been extracted according to the location of the V-notch with regards to weld bed in the parent tube (Fig. 2): a base metal notched specimen (BMS), a fusion zone notched specimen (FZS), and a heat-affected zone specimen (HAZS). Then, for each specimen type, two series of production processes have been used: a series of machined specimens and a series of machines and surface-treated specimen. The V-notch is added using a specific notch cutting tool before conducting impact tests from 50 to −60 °C with increments of 20 °C.

The surface treatment of impact specimens has been achieved mechanically using a ball burnishing tool on a vertical milling machine. So a purpose burnishing tool has been designed as shown in Fig. 3. The system consists of a hard steel ball that is mounted on a shaft that slides in a hub of the tool holder. The applied force is calibrated with a specific load spring. The burnishing system is mounted on the spindle to be subjected to vertical displacement. The burnishing operation consists of first applying a pressure with a ball on the surface of a part as to get a corresponding plastic deformation on a point of the external layer and then scanning the ball through the whole surface to be burnished.

2.2.3 Hardness tests

Exploratory hardness measurements have been conducted on center weld bed impact specimens according to the ASTMA370 standard equivalent to API 5L 45 Ed (Fig. 4a). Hardness tests have been made on different located points in the base metal zone, fusion zone, and heat-affected zone. Figure 4b shows a view of impact specimen under Vickers indentation using a Vickers matzuzawaMXT70 microindenter with a load of 500 gf. The investigation concerned both machined specimen and burnished specimen.

3 Results and discussion

3.1 Effect of weld bed on tensile properties

Results of tensile tests on base metal specimens and weld bed specimens are illustrated in Fig. 5. As expected, the general stress strain curve behavior is observed for both conditions. A

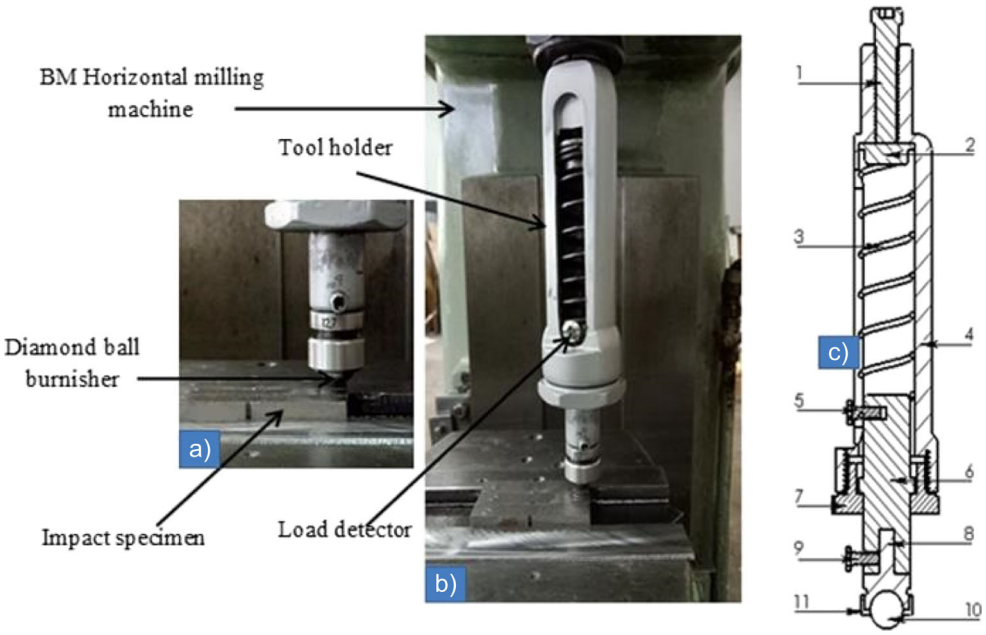

Fig. 3 Ball burnishing tool device for MST of impact specimens. **a** Photograph of active part; **b** burnishing tool mounted on the horizontal milling machine; **c** detailed sectional burnishing tool device assembly. 1—adjusting screw, 2—spring bed, 3—spring, 4—tool holder, 5—load detector, 6—shaft, 7—shaft holder, 8—ball holder, 9—tightening screw, 10—artificial diamond ball, and 11—ball nut

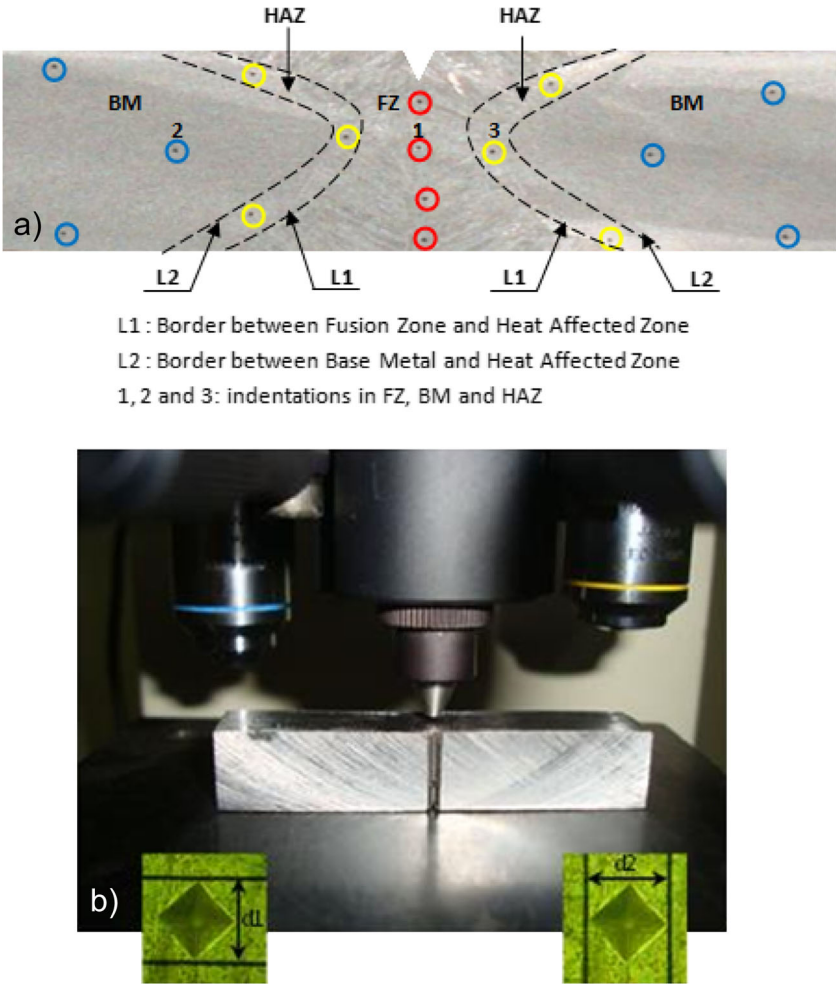

Fig. 4 Hardness measurement according to API 5L 45 Ed. **a** Location of hardness measuring points; **b** view of impact specimen for hardness tests

ductile behavior is obtained with a strain up to 32% for the base metal specimens and 22% for the weld bed specimens. The morphology of the fracture surface shows that the necking area occurred in base metal in both specimens (Fig. 6). Basically, a conventional mode I fracture characterized by a shearing slope is observed in the middle distance of the gauge length for the BM specimen and far from the weld bed, at the beginning of the gauge length for the weld bed specimen. However, in some BM specimen, the fracture occurred following two modes of fracture: mode I and mode II (Fig. 6a). Meanwhile, the base metal is more ductile and presented higher values of tensile properties as summarized in Table 3, showing good agreement with the API standard requirement values. Comparing to results in base metal, the elastic modulus in the weld bed case has increased to 1.07 times and the yield strength (σ_y) and the σ_{ts} have decreased to about 0.86 and 0.89 times. The tensile properties do not affect the global resistance of the material, and even more, the fracture occurred away from the weld bed as the cross section in the weld bed is greater than that in the base metal. Nevertheless, the fracture toughness should decrease when approaching the weld joint.

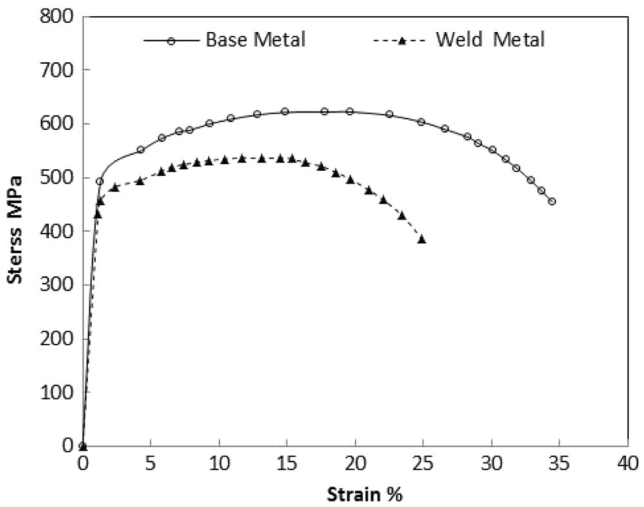

Fig. 5 Stress strain curves in API X70 spiral welded pipe

3.2 Effect of mechanical treatment on hardness

Mechanical treatment has been achieved using ball burnishing on a vertical milling machine (Fig. 3). The burnishing operation

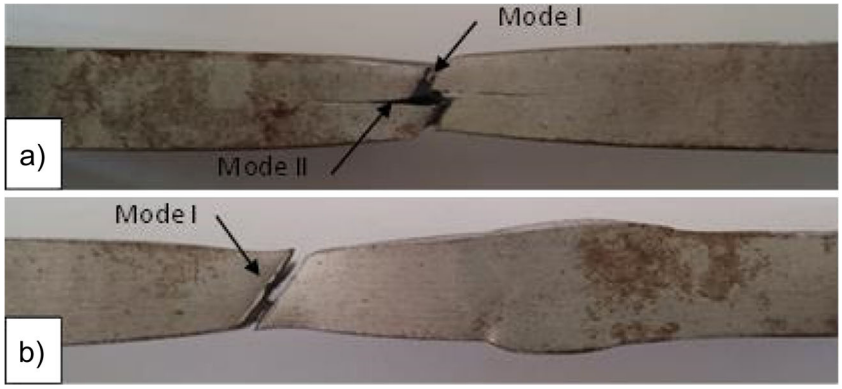

Fig. 6 Conventional shearing slope in the tensile fracture API 70 specimens. **a** Base metal specimen; **b** weld bed specimen

Table 3 Tensile mechanical properties in API X70 spiral welded pipe

Type of specimen	E (GPa)	$\sigma_{y0.5}$ (MPa)	σ_{ts} (MPa)
Base metal	193	493	622
Weld joint	207	478	537
API X 70 requirements	190–220	485–635	531–758

was not possible on the tensile specimens because of the complexity of the geometrical configuration of the specimen particularly for weld joint ones. Therefore, one solution is conducting investigation of the ball burnishing through measurements of hardness on impact V-notch specimens. Figure 7 shows the morphology of the surface-ball-burnished specimen. Figure 7a shows the state of a machine-milled surface where the strips left by the passage of the milling tool are observed. Figure 7b shows the effect of ball burnishing on a machine-milled surface. The morphology illustrates the circular marks of the passage of the ball burnishing tool. The pressure of the ball on the surface generates surface deformations that are intersecting together after each run away of the ball.

Hardness measurement results are given in Table 4. Figure 8 shows the indentation geometry in the weld zone. The distance between adjacent indentations has been at least three times greater than the diameter of the indentation in order to avoid the effect of plastic deformation around the indentation. Figure 9 illustrates a histogram plot of the respective mean values of six measurements in the three zones of center notched impact specimens, revealing the effect of ball burnishing. There is a slight difference between the measured values. In the base metal, hardness is 246; it increased in the fusion zone to 283 and decreased to 268 in the heat-affected zone. This has been expected as heat-generated welding is high in the fusion zone which obviously will take longer to cool down, and the base zone will cool faster. The heat-affected zone will be subjected to a competition in cooling faster because of the base zone's lower temperature and the fusion zone's higher temperature. By the time the fusion zone cools down to room temperature, the affected zone will become softer. When introducing ball burnishing, hardness drops slightly down in the three zones showing softer material where hardness decreased by 1.016, 1.029, and 1.05 times respectively for the BM, FZ, and HAZ. However, the small difference is very representative when regarding the evolution of fracture toughness as discussed in next feature.

3.3 Effect of mechanical treatment on absorbed energy

Fracture results for both as-machined specimens and ball-burnished specimens are shown in Fig. 10 that represent plots of Charpy absorbed energy versus temperature. In all specimens, the general steel fracture behavior at low temperatures is observed as the material becomes brittle. The energy

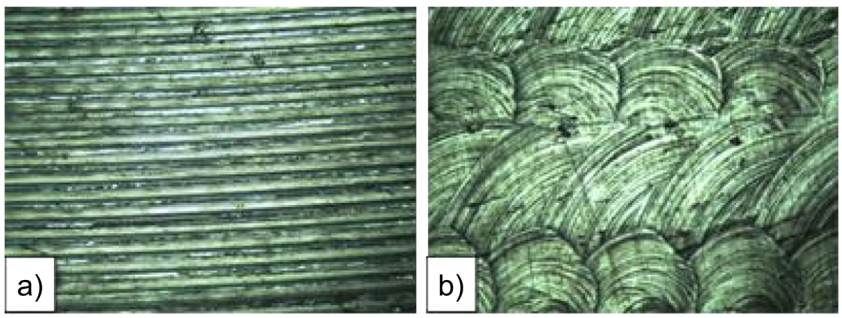

Fig. 7 Morphology of machined specimen (**a**) and burnished specimen (**b**)

Table 4 Hardness measurement according to API 5L 45 Ed

No.	Machined specimen			Burnished specimen		
	BM	ZF	HAZ	TBM	TZF	THAZ
1	213	263	257.6	226.5	254.6	253.8
2	243.8	295.6	272.4	223.7	284	252.9
3	225.8	286.4	272.8	238	274.4	257.2
4	246.6	291.5	255.1	249.7	280.8	244.2
5	272.8	283	283.3	260.9	298.4	251.9
6	276.3	282.1	270.3	254.1	263.1	273.1
Mean value	246.3	283.6	268.5	242.1	275.8	255.5

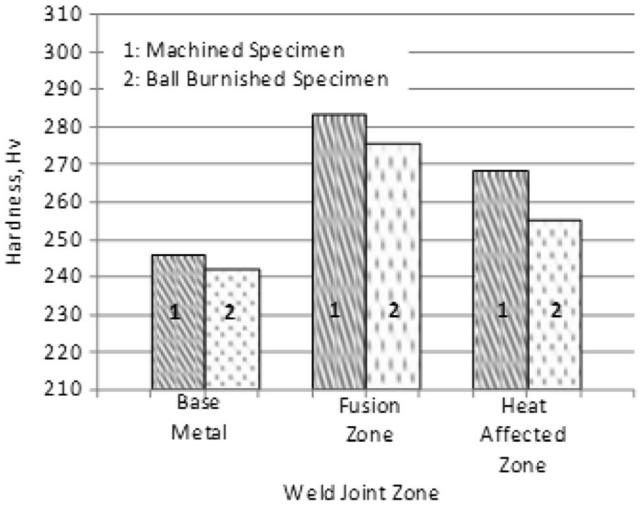

Fig. 9 Effect of ball burnishing on hardness in impact test specimens

decreases as the testing temperature is decreased from 50 to −60 °C. In addition, the transition temperature from ductile to brittle is found to be starting from −40 °C. Further drop in temperature leads to the convergence of the three curves to the same transition slope. Above 40 °C, there is a change when the curves followed a knee-shape profile as the testing temperature increases.

In the machined conditions (Fig. 10a), both heat zones, ZF and HAZ, showed a knee-shape profile starting very soon and were completed at a temperature of −20 °C where the respective values of knee absorbed energy (Kv) were 168 and 178 J. In the BM zone, the slope of the fracture curve reduces progressively until the temperature reached 0 °C where a knee-shape profile appeared with Kv of 248 J. Then, the three curves continued to progress from the knee zone almost with a very small slope approaching an angle of 0° as the temperature reached 0 °C. The main observation is that when the temperature is decreased from 50 to −40 °C corresponding to the start of the transition temperature, the base metal showed better fracture resistance, for instance at a temperature of 20 °C of respectively 1.18 and 1.25 times higher than that in the FZ and HAZ metals.

In the ball-burnished conditions, the most interesting phenomenon is observed in the change of the trend of the three curves between 20 and −40 °C. In fact, the BM curve formed a first knee-shape profile from Kv equals to 278 J and sloped rapidly down as the testing temperature is decreased to −20 °C where the curve regained a slight slope to show a second knee-shape profile where Kv is 152 J. Meanwhile, the FZ and HAZ absorbed energy curves jumped up above the BM energy curve as the testing temperature falls from 2 to −60 °C. The FZ curve showed two knee-shape profiles at −40 °C where the Kv was 158 J and at about 0 °C with Kv of 215 J.

In both conditions, at 20 °C, Kv values corresponded to the measured hardness values. Where hardness is high, Kv is low, and as the hardness given by the ball burnishing process decreased, the absorbed energy increases, making the metal more resistant to brittle fracture and vice versa.

The absorbed energy in BM was high, and in the FZ and HAZ, it decreased even more for ball-burnished specimens. However, the most interesting phenomena are observed in the curves of the absorbed energy vs temperature between the transition temperature of − 40 °C and room temperature of 20 °C. SEM observations revealed that ball burnishing affects also the core of the impact specimens.

3.4 Fracture surface observations

Surface fracture and SEM observations have been made using a FEI Quanta 250 microscope on the surface of broken impact specimens in order to understand the behavior of the material in response to fracture. Fracture surface observations at room temperature on as-machined specimens and on burnished specimens are shown in Fig. 11.

In the as-machined impact specimens (Fig. 11a, b), the specific ductile fracture mode of X70 steel is observed.

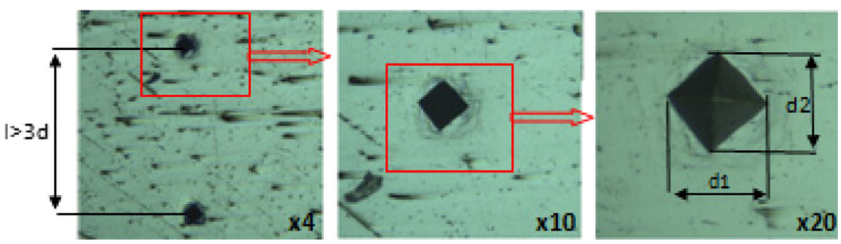

Fig. 8 Indentation geometry in the fusion zone

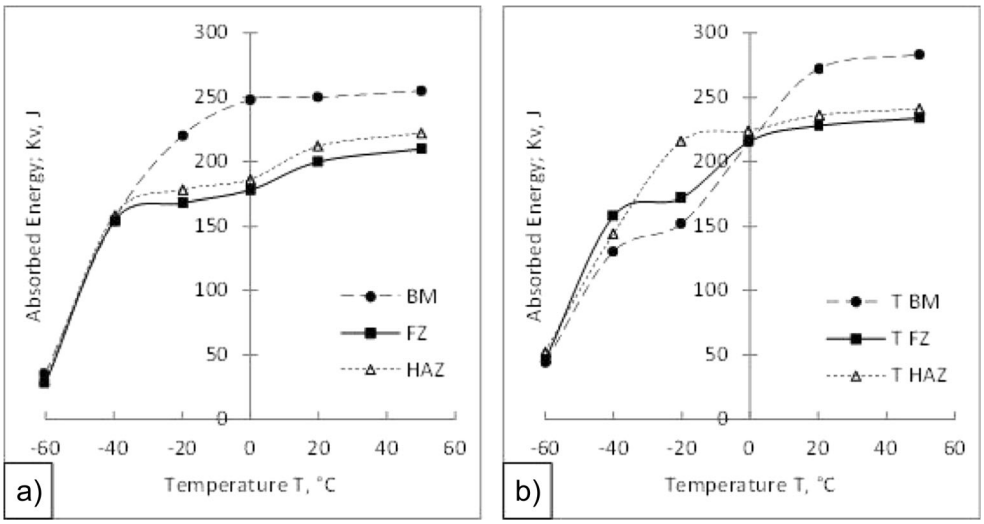

Fig. 10 Effect of temperature on absorbed energy in machined specimens (**a**) and in burnished specimens (**b**)

Dimples from micro void coalescence appearing in the fractography can be considered as evidence of ductile material. In the BM (Fig. 10b), dimples have medium size; in the FZ, they are shallow and fine; and in the HAZ, they are large and deep. The tear dimples were generated by the nonuniform distribution of the stress at the crack tip in the V-notched impact specimens (Fig. 12). There were a lot of abnormal spherical bodies that were resulted from the

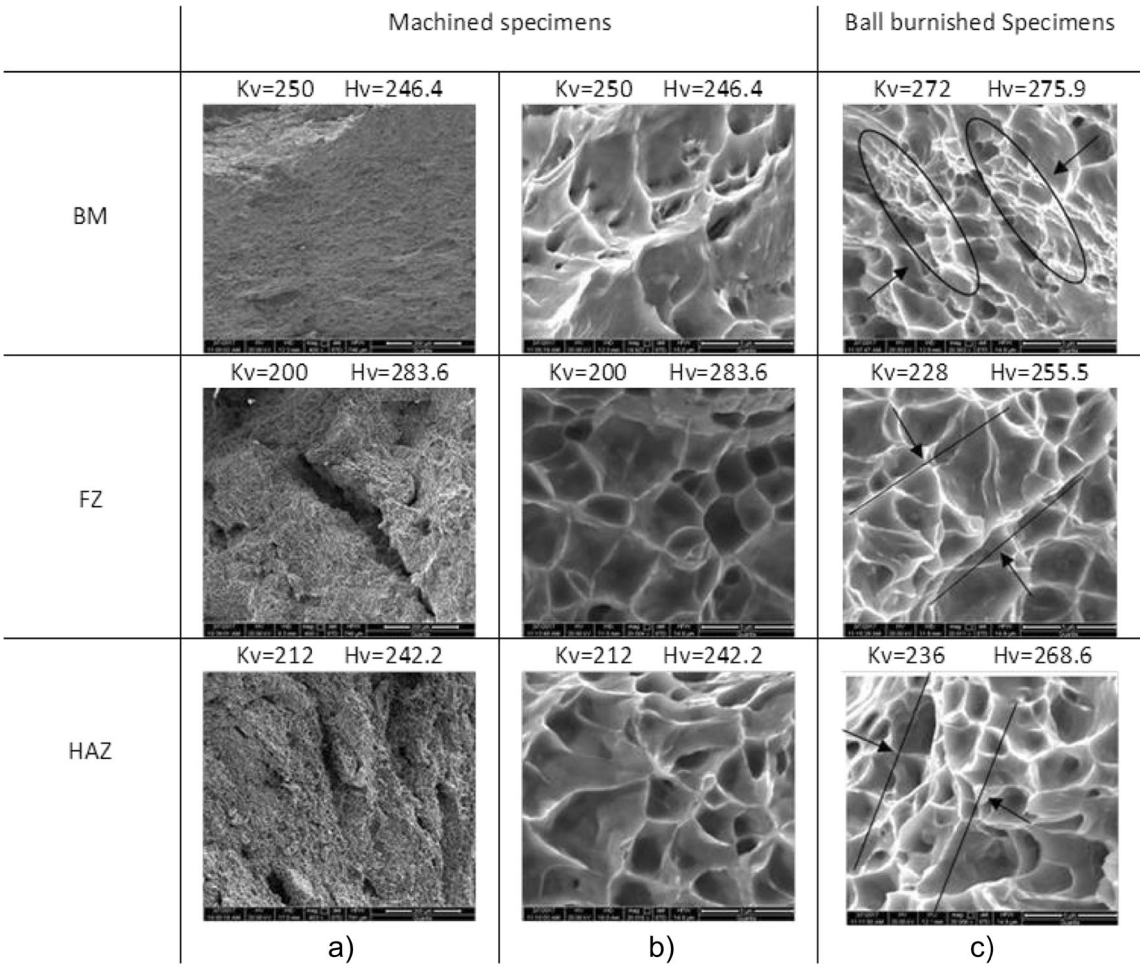

Fig. 11 View of SEM fractographies in the center of different impact specimens. (The arrows in Fig. 10c show the direction of the applied ball burnishing load)

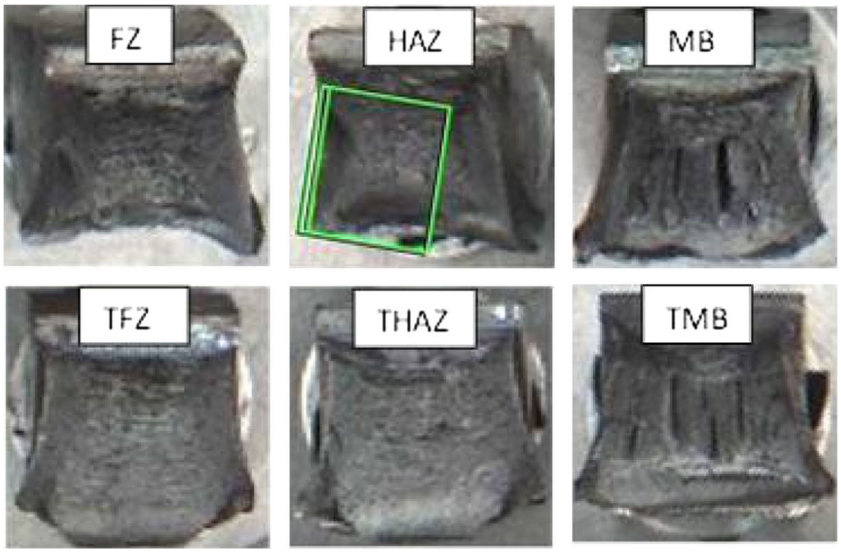

Fig. 12 Eye view on fracture surface in machined and ball-burnished impact specimens

precipitates caused by the welding heat. Accordingly, the toughness of BM absorbed energy higher than that of FZ and HAZ which is in good agreement with results given in Fig. 10.

In the ball-burnished specimens (Fig. 11c), there is a significant effect of the ball pressure on the fracture surface. As the specimens are 10 mm thick, the applied pressure has not only affected the surface of the specimen, but resulted in deep change of the structure that is compressed as to stretch the grains along the perpendicular direction to the applied load. This resulted in a remarkable change that is specific to each metal zone. In the BM, the open and spacious structure became dense with concentrated grains and dimples in the center of the specimen. In the FZ, the shallow and fine dimples stretched and moved along as to form a sort of river bed shape demonstrating that ball burnishing has a great effect in redeveloping the repartition of the grains and dimples. In the HAZ, similar phenomena occurred and the dimples are no larger within the center of the specimen as they have been pushed together taking greater length in the perpendicular direction to the applied load.

4 Conclusion

The present investigation concerned the effect of ball burnishing on fracture toughness in API X70 pipeline steel. First, the mechanical properties of the material are determined according to the process of pipeline production. Then, absorbed energy from the impact test specimens is determined in both the as-machined and ball-burnished specimens. The main conclusions are summarized below.

As expected, the general stress strain curve behavior is observed for both and welded material, showing the material is ductile.

Hardness measurement revealed the effect of ball burnishing. There is a slight difference between the measured values but the BM is less hard. When introducing ball burnishing, hardness drops slightly down showing softer material by a maximum of 1.0024 times for the base metal.

In all the specimens, the general steel fracture behavior at low temperatures is observed as the material becomes brittle. The most interesting phenomenon is that observed in the change of the trend of the three curves, BM, FZ and HAZ, between 20 and −40 °C for both as-machined and ball-burnished specimens. Above 20 °C and below −40 °C corresponding to the transition slope, the trend of the absorbed energy vs temperature was almost the same.

SEM surface fracture observations revealed that applying ball burnishing on impact specimens affected both the surfaces and the core of the impact specimens.

Acknowledgments The authors would like to thank the metallurgy laboratory of Badji Mokhtar University Annaba for specimen preparation, hardness measurements, and metallographic observations. Thanks are due to the staff of mechanical laboratory of Alfapipe of the Algerian steel company in El-Hadjar, Annaba, for the furniture of the material and the preparation of tensile and impact specimens and also conducting the corresponding mechanical tests. Thanks to URASM, the applied research unit in welding and metallurgy of Annaba, for analyzing the composition of the material. A great thank to ENSMM, the Algerian national high school of mining and metallurgy in Annaba, for their contribution in SEM observations.

Nomenclature A%, ultimate elongation (%); BM, base metal; d1, distance on one diagonal of a diamond print (mm); d2, distance on the second diagonal of a diamond print (mm); E, Young modulus (GPa); FZ, fusion zone; HAZ, heat-affected zone; HSLA, high-strength low-alloy steel; HSS, high-

strength steel; Hv, Vickers hardness; Kv, absorbed energy (J); SEM, scanning electron microscope; TBM, treated base metal; TFZ, treated fusion zone; THAZ, treated heat-affected zone; $\sigma_{y0.5}$, yield strength (MPa); σ_{ts}, tensile strength (MPa)

References

1. Zelmati D, Ghelloudj O, Amirat A (2016) Reliability estimation of pressurized API 5L X70 pipeline steel under longitudinal elliptical corrosion defect. Int J AdvManuf Technol. https://doi.org/10.1007/s00170-016-9580-6
2. Richards, F. (2013). Failure analysis of a natural gas pipeline rupture, 653–657. https://doi.org/10.1007/s11668-013-9745-7
3. Yang X, Xu Y, Tan X, Wu D (2014) Influences of crystallography and delamination on anisotropy of Charpy impact toughness in API X100 pipeline steel. Mater Sci Eng A 607:53–62. https://doi.org/10.1016/j.msea.2014.03.121
4. Yang X, Xu Y, Tan X, Wu D (2015) Relationships among crystallographic texture, fracture behavior and Charpy impact toughness in API X100 pipeline steel. Mater Sci Eng A 641, 96:–106. https://doi.org/10.1016/j.msea.2015.06.029
5. Chen, X., Lu, H., Chen, G., and Wang, X. (2015). A comparison between fracture toughness at different locations of longitudinal submerged arc welded and spiral submerged arc welded joints of API X80 pipeline steels, Department of Mechanical and Aerospace Engineering, Carleton University, Ottawa, ENGINEERING FRACTURE MECHANICS. https://doi.org/10.1016/j.engfracmech.2015.09.003
6. Hwang B, Shin SY, Lee S, Kim NJ, Kim S, Kang KB (2006) Correlation of crack-tip opening angle for stable crack propagation with Charpy and drop-weight tear test properties in high-toughness API X70 pipeline steels. Metall Mater Trans A Phys Metall Mater Sci 37(2):371–380. https://doi.org/10.1007/s11661-006-0007-0
7. Yong, S., Hwang, B., Kim, S., and Lee, S. (2006). Fracture toughness analysis in transition temperature region of API X70 pipeline steels, 429, 196–204. https://doi.org/10.1016/j.msea.2006.05.086
8. Shin SY, Gong G, Kim S, Lee S (2007) Analysis of fracture toughness in the transition temperature region of API X70 pipeline steels rolled in two-phase region. Metall Mater Trans A Phys Metall Mater Sci 38(5):1012–1021. https://doi.org/10.1007/s11661-007-9125-6
9. Materials, E. (2009). On the relation of microstructure and impact toughness characteristics of DSAW steel of grade API X70. Fatigue Fract Eng Mater Struct, 33–40. https://doi.org/10.1111/j.1460-2695.2008.01312.x
10. Park D, Gravel J (2015) Fracture toughness measurements using two single-edge notched bend test methods in a single specimen. Eng Fract Mech 144:78–88. https://doi.org/10.1016/j.engfracmech.2015.06.033
11. Maheshwari, A. S., and Gawande, R. R. (2017). Influence of specially designed high-stiffness ball burnishing tool on surface quality of Titanium alloy. Materials Today: Proceedings, ScienceDirect 4(2), 1405–1413. https://doi.org/10.1016/j.matpr.2017.01.162
12. Liu, Z. Y., Fu, C. H., Sealy, M. P., Zhao, Y., and Guo, Y. B. (2017). Benchmark burnishing with Almen strip for surface integrity, 10, 456–466.https://doi.org/10.1016/j.promfg.2017.07.027
13. Shiou F, Huang S, Shih AJ, Zhu J, Yoshino M (2017) Fine surface finish of a hardened stainless steel using a new burnishing tool. Proc Manuf 10:208–217. https://doi.org/10.1016/j.promfg.2017.07.048
14. Yuan X, Sun Y, Li C, Liu W (2017) Experimental investigation into the effect of low plasticity burnishing parameters on the surface integrity of TA2. Int J Adv Manuf Technol:1089–1099. https://doi.org/10.1007/s00170-016-8838-3
15. Hamadache, H., Zemouri, Z., Laouar, L., and Dominiak, S. (2014). Improvement of surface conditions of 36 Cr Ni Mo 6 steel by ball burnishing process, 28(4), 1491–1498. https://doi.org/10.1007/s12206-014-0135-1
16. Chomienne V, Valiorgue F, Rech J, Verdu C (2016) Influence of ball burnishing on residual stress profile of a 15-5PH stainless steel. CIRP J Manuf Sci Technol. https://doi.org/10.1016/j.cirpj.2015.12.003
17. Amdouni H, Bouzaiene H, Montagne A, Van Gorp A, Coorevits T, Nasri M, Iost A (2016) Experimental study of a six new ball-burnishing strategies effects on the Al-alloy flat surfaces integrity enhancement. Int J AdvManuf Technol. https://doi.org/10.1007/s00170-016-9529-9
18. Korhonen H, Laakkonen J, Hakala J, Lappalainen R (2013) Improvements in the surface characteristics of stainless steel work pieces by burnishing with an amorphous diamond-coated tip. Mach Sci Technolo 17:593–610
19. Devaraya, G., Shetty, R., and Srinivas, S. (2016). Wear resistance enhancement of titanium alloy (Ti–6Al–4V) by ball burnishing process. Integrative Medicine Research, (x x). https://doi.org/10.1016/j.jmrt.2016.03.007
20. Grocha D, Berczy S, Grz Z (2017) Modeling of burnishing thermally toughened X42CrMo4 steel with a ceramic ZrO 2 ball. ScienceDirect 7:2–9. https://doi.org/10.1016/j.acme.2017.04.009
21. Avilés, R., Albizuri, J., Rodríguez, A., and De Lacalle, L. N. L (2013). Influence of low-plasticity ball burnishing on the high-cycle fatigue strength of medium carbon AISI 1045 steel, *55*, 230–244. https://doi.org/10.1016/jijfatigue201306024
22. Yuan X, Sun Y, Li C (2017) An engineering high cycle fatigue strength prediction model for low plasticity burnished samples. Int J Fatigue. https://doi.org/10.1016/j.ijfatigue.2017.06.013
23. Okada M, Shinya M, Matsubara H, Kozuka H, Otsu M (2017) Development and characterization of diamond tip burnishing with a rotary tool. J Mater Process Technol 244:106–115
24. Shiou, F., and Banh, Q. (2016). Development of an innovative small ball-burnishing tool embedded with a load cell, (43). https://doi.org/10.1007/s00170-016-8413-y
25. He, D., Wang, B., Zhang, J., Liao, S., and Deng, W. J. (2017). Investigation of interference effects on the burnishing process. https://doi.org/10.1007/s00170-017-0640-3
26. Hiegemann L, Weddeling C, Tekkaya AE (2016) Analytical contact pressure model for predicting roughness of ball burnished surfaces. J Mater Process Tech. https://doi.org/10.1016/j.jmatprotec.2016.01.024